A&A 526, L9 (2011)
DOI: 10.1051/0004-6361/201016119

Astronomy & Astrophysics

Letter to the Editor

The *XMM* Deep survey in the CDF-S

I. First results on heavily obscured AGN⋆,⋆⋆

A. Comastri[1], P. Ranalli[2,1], K. Iwasawa[3,1], C. Vignali[2,1], R. Gilli[1], I. Georgantopoulos[1], X. Barcons[4], W. N. Brandt[5,6], H. Brunner[7], M. Brusa[7,8], N. Cappelluti[1,8], F. J. Carrera[4], F. Civano[9], F. Fiore[10], G. Hasinger[11], V. Mainieri[12], A. Merloni[7], F. Nicastro[10,9], M. Paolillo[13], S. Puccetti[14], P. Rosati[11], J. D. Silverman[15], P. Tozzi[16], G. Zamorani[1], I. Balestra[7], F. E. Bauer[17], B. Luo[5], and Y. Q. Xue[5]

[1] INAF – Osservatorio Astronomico di Bologna, via Ranzani 1, 40127 Bologna, Italy
e-mail: andrea.comastri@oabo.inaf.it
[2] Dipartimento di Astronomia, Università di Bologna, via Ranzani 1, 40127 Bologna, Italy
[3] ICREA and Institut de Ciències del Cosmos, Universitat de Barcelona (IEEC-UB), Martí i Franqués 1, 08028 Barcelona, Spain
[4] Instituto de Física de Cantabria (CSIC-UC), Avenida de los Castros, 39005 Santander, Spain
[5] Department of Astronomy and Astrophysics, 525 Davey Lab, the Pennsylvania State University, University Park, PA 16802, USA
[6] Institute for Gravitation and the Cosmos, The Pennsylvania State University, University Park, PA 16802, USA
[7] Max-Planck-Institut für extraterrestrische Physik, Giessenbachstrasse 1, 85748 Garching bei München, Germany
[8] University of Maryland, Baltimore County, 1000 Hilltop Circle, Baltimore, MD 21250, USA
[9] Harvard-Smithsonian Center for Astrophysics, 60 Garden Street, Cambridge, MA 02138, USA
[10] INAF – Osservatorio Astronomico di Roma, via Frascati 33, 00040 Monteporzio Catone, Italy
[11] Max-Planck-Institut für Plasmaphysik, Boltzmannstrasse 2, 85748 Garching bei München, Germany
[12] European Southern Observatory, Karl-Schwarzschild-Strasse 2, 85748 Garching bei München, Germany
[13] Dipartimento di Scienze Fisiche, Università di Napoli "Federico II," V. Cinthia 9, 80126 Napoli, Italy
[14] ASI Science Data Center, via Galileo Galilei, 00044 Frascati, Italy
[15] Institute for the Physics and Mathematics of the Universe (IPMU), IPMU, University of Tokyo, Kashiwanoha 5-1-5, Kashiwa, Chiba 277-8568, Japan
[16] INAF – Osservatorio Astronomico di Trieste, via Tiepolo 11, 34143 Trieste, Italy
[17] Pontificia Universidad Católica de Chile, Departamento de Astronomía y Astrofísica, Casilla 306, Santiago 22, Chile

Received 10 November 2010 / Accepted 16 December 2010

ABSTRACT

We present the first results of the spectroscopy of distant, obscured AGN as obtained with the ultra-deep (≈3.3 Ms) *XMM-Newton* survey in the *Chandra* deep field South. One of the primary goals of the project is to characterize the X-ray spectral properties of obscured and heavily obscured *Compton*-thick AGN over the range of redhifts and luminosities that are relevant in terms of their contribution to the X-ray background. The ultra-deep exposure, coupled with the *XMM* detector's spectral throughput, allowed us to accumulate good quality X-ray spectra for a large number of X-ray sources and, in particular, for heavily obscured AGN at cosmological redshifts. Specifically we present the X-ray spectral properties of two high-redshift – $z = 1.53$ and $z = 3.70$ – sources. The *XMM* spectra of both are very hard, with a strong iron Kα line at a rest-frame energy of ∼6.4 keV. A reflection-dominated continuum provides the best description of the X-ray spectrum of the $z = 1.53$ source, while the intrinsic continuum of the $z = 3.70$ AGN is obscured by a large column $N_{\rm H} \approx 10^{24}$ cm^{-2} of cold gas. *Compton*-thick absorption, or close to it, is unambiguously detected in both sources. Interestingly, these sources would not be selected as candidate Compton thick AGN by some multiwavelength selection criteria based on the mid-infrared to optical and X-ray to optical flux ratios.

Key words. galaxies: active – galaxies: high-redshift – X-rays: galaxies – X-rays: diffuse background

1. Introduction

The deepest X-ray surveys ever performed with the *Chandra* satellite in the *Chandra* Deep Field North (CDF-N, Alexander et al. 2003) and *Chandra* Deep Field South (CDF-S, Luo et al. 2008) have reached extremely faint X-ray fluxes (≈2 × 10^{-17} erg cm^{-2} s^{-1} in the 0.5–2 keV band) and X-ray source surface densities of ≈10 000 per square degree. Both ultra-deep *Chandra* fields cover relatively small areas of the sky (about 440 arcmin^2 each), and the majority of the sources are detected with a number of counts that prevents a detailed X-ray spectral analysis.

The ultra-deep *XMM-Newton* survey, with a nominal exposure of almost 3 Ms over an area encompassing the CDF-S and most of its four flanking fields (E-CDF-S), was conceived and planned to increase the counting statistics for a large number of X-ray sources, thanks to the large spectral throughput of *XMM-Newton*, and thus complements the *Chandra* and multi-wavelength surveys information in that portion of the sky.

The primary goal of the *XMM-Newton* ultra-deep survey in the CDF-S is the study of the X-ray spectral properties and

⋆ This work is based on observations obtained with *XMM-Newton*, an ESA science mission with instruments and contributions directly funded by ESA Member States and the USA (NASA).
⋆⋆ Table 1 is only available in electronic form at http://www.aanda.org

cosmological evolution of heavily obscured and *Compton*-thick ($N_{\rm H} \gtrsim 10^{24}$ cm^{-2}, hereafter CT, see Comastri 2004, for a review) AGN. In recent years it has become clear that nuclear obscuration may be associated with a specific, early phase in the cosmic history of every AGN (e.g. Page et al. 2004; Hopkins et al. 2006; Menci et al. 2008). At high redshift, the large gas reservoir may be able to both fuel and obscure the accreting supermassive black hole (SMBH) and sustain vigorous star formation in the host galaxy. A sizable population of heavily obscured CT AGN at the redshift peak of AGN activity ($z \sim 1-2$) is also invoked to reconcile the local SMBH mass function with that obtained from the AGN luminosity function (Marconi et al. 2004).

The space density of obscured AGN beyond the local Universe is estimated by subtracting the cumulative flux and spectrum of resolved sources from the total X-ray background (XRB) intensity (Worsley et al. 2004; Comastri et al. 2005) or in the framework of population synthesis models for the XRB (e.g. Gilli et al. 2007; Treister & Urry 2005). Following the approach described above, the most promising candidates to explain the so far largely unresolved spectrum of the XRB around its 20–30 keV peak are heavily obscured ($N_{\rm H} > 10^{23}$ cm^{-2}) AGN at $z \sim 0.5-1.5$, many of them being CT. The integral contribution of CT AGN to the hard (>10 keV) XRB and in turnto the cosmic SMBH accretion history depends on the assumptions made in the synthesis models and ranges from about 10% (Treister et al. 2009) up to ~30% (Gilli et al. 2007). These estimates are made under simplified hypotheses, because the lack of observational evidence about the cosmological evolution and the spectral shape of the most obscured AGN. It is customary to constrain the CT AGN local space density by requiring that it matches the results obtained for optically selected (Risaliti et al. 1999; Guainazzi et al. 2005) or hard X-ray selected Swift (Tueller et al. 2010) and INTEGRAL (Beckmann et al. 2009) surveys in the local Universe.

At present, only a handful of the "bona fide" known CT AGN (Comastri 2004; Della Ceca et al. 2008) have been found at cosmological distances (Norman et al. 2002; Iwasawa et al. 2005; Alexander et al. 2008) by means of X-ray observations. A systematic search for X-ray selected CT AGN has been carried out in the CDF-S (Tozzi et al. 2006) and CDF-N (Georgantopoulos et al. 2009) yielding several candidates spanning a broad redshift range (up to $z = 3.7$). The surface density of the candidate CT AGN agrees fairly well with the Gilli et al. (2007) XRB synthesis model predictions. Though effective in finding the signature of heavy obscuration, *Chandra* surveys are limited in photon-counting statistics. The CT nature of most of the candidates is inferred on the basis of relatively poor quality (less than a few hundred counts) X-ray spectra. For this reason, alternative, multi-wavelength selection techniques based on high-ionization, narrow optical emission lines (Vignali et al. 2010; Gilli et al. 2010) or on the ratio between mid-infrared and optical fluxes (Daddi et al. 2007; Alexander et al. 2008; Fiore et al. 2008, 2009) were developed in the last few years. They seem to be promising to find sizable samples of highly obscured and/or CT AGN at moderate to high redshifts ($z \sim 1-3$). However, they rely on indirect methods, such as stacking, and may still be prone to contamination by less obscured AGN or galaxies (e.g. Donley et al. 2008).

The ultra-deep *XMM-Newton* exposure over an area covering the CDF-S and its flanking fields coupled with the spectral throughput of the *pn* and MOS detectors is expected to deliver X-ray spectra of unprecedented quality and thus to unambiguously identify CT absorption signatures in a significant number of objects. In this paper (Paper I) we give an overview of the *XMM-Newton* survey in the CDF-S field and present the X-ray spectral analysis of two obscured AGN. We adopt a cosmology with $H_0 = 70$ km s^{-1} Mpc^{-1}, $\Omega_{\rm M} = 0.3$, $\Omega_\Lambda = 0.7$.

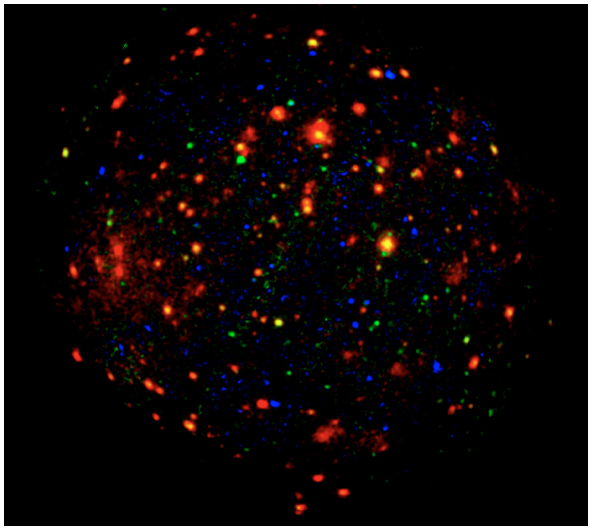

Fig. 1. Combined *pn* and MOS color image. The standard color-coding is adopted: red for the soft (0.4–1 keV) band, green for the medium (1–2 keV) band and blue for the hard (2–8 keV) band. The energy range around the strong copper line at 7.8 keV in the *pn* data is removed. The image size is ≈32′ on a side and has been smoothed with a 4 arcsec Gaussian kernel.

2. Observations and data analysis

The CDF-S area was surveyed with *XMM-Newton* in several different epochs spread over almost nine years. The results presented in this paper are obtained combining the observations awarded to our project in AO7 and AO8 (and performed in four different epochs between July 2008 and March 2010, with the archival data obtained in the period July 2001–January 2002). The total exposure after cleaning from background flares is ≈2.82 Ms for the two MOS and ≈2.45 for the *pn* detectors. An extended and detailed description of the full data set including data analysis and reduction and the X-ray catalog will be published in Ranalli et al. (in prep.).

The data reduction was carried out with the standard *XMM-Newton* data analysis software SAS 9.0 and HEASARC's FTOOLS. The event files used for extracting spectra were filtered by applying light curves of the whole field in the high-energy band where few source photons are expected: 10–12 keV for the *pn* and 9.5–12 keV for the MOS, and the quiescent time intervals were selected. Background flares were filtered with a 3σ clipping procedure. Individual pointings were slightly off-set from each other to smear detector gaps and obtain a more uniform coverage of the field. *pn* observations are more affected by "high" particle background periods and detector gaps than MOS; as a consequence, the net *pn* exposure time is significantly shorter than for MOS. The individual pointings were brought to a common reference frame using the positions of the *Chandra* sources (Luo et al. 2008). X-ray images in soft (0.4–1 keV), medium (1–2 keV) and hard (2–8 keV) bands were accumulated for each orbit and summed. The color image is shown in Fig. 1.

3. X-ray spectral properties of two high-redshift obscured AGN

A sample of 14 candidate CT AGN from the CDF-S *Chandra* 1 Ms observations was selected by Tozzi et al. (2006) on the

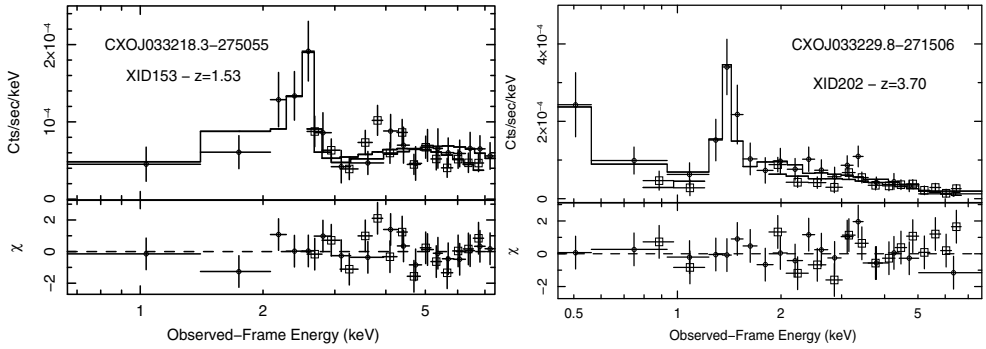

Fig. 2. Best-fit spectra and residuals of XID 153 (*left panel*) and XID 202 (*right panel*). *pn* and MOS data are plotted as circles and squares, respectively. The spectra were mildly rebinned for plotting purposes.

basis of a flat hard X-ray spectrum typical of reflection-dominated sources. The presence of a strong (*EW* of the order of 1 keV) iron Kα line is considered as additional evidence of heavy, *Compton*-thick obscuration.

We present the *XMM-Newton* spectral analysis of two objects from the parent sample described above: CXOCDFSJ033218.3-275055 at $z = 1.53$ and CXOCDFSJ033229.8-275106 at $z = 3.7$ (XID 153 and XID 202, respectively, in the numbering scheme of Giacconi et al. 2002). The former is the brightest X-ray source of the *Chandra* sample of candidate CT AGN, while the latter is the highest redshift heavily obscured AGN known to date in the CDF-S (Norman et al. 2002).

For each individual *XMM* orbit, source counts were collected from a circular region of 15 arcsec radius, centered on the source position. Local background data were taken from a nearby region, where no source is found in the full exposure image or in the *Chandra* 2 Ms observations. The area of the background region is larger than the source region by a factor of 1.7. The spectral data from individual exposures were summed up for the source and background, respectively, and the background subtraction was made assuming the common scaling factor for the source/background geometrical areas. *pn* spectra are extracted in the 0.5–7.8 keV energy range to avoid the strong ~8 keV Cu line. Above ~8 keV, the signal-to-noise ratio decreases rapidly for relatively faint sources. MOS spectra are extracted in the 0.5–9 keV range. X-ray photons in the 1.2–1.8 keV range in the MOS are discarded to avoid instrumental background features and in particular the ≈1.5 keV Al line. MOS1 and MOS2 spectra are summed. Response and effective area files were computed by averaging the individual files for each orbit. *pn* and MOS spectra were rebinned requiring at least 30 net counts per channel and fitted simultaneously leaving the normalization free to vary. The *pn* count spectra are shown in Fig. 2. There is no clear evidence of significant flux or spectral variability between observations taken a few years apart. Variability studies on shorter timescales are hampered by the limited counting statistic.

Spectral fits are first performed with a single power law plus a Gaussian line. This modeling is purely phenomenological and meant as a guide for more complex fits, which are summarized in Table 1. We consider either a reflection-dominated continuum or a power law plus intrinsic absorption, partially or totally covering the central source. In all fits a narrow (below the intrinsic instrumental energy resolution) iron line at ~6.4 keV is included. Errors are quoted at the 1σ confidence level for one parameter of interest.

3.1. CXOCDFSJ033218.3-275055 (XID 153) z = 1.53

The *pn* exposure time is about 1683 ks, after flare screening while the average MOS exposure time is about 2618 ks. The net counts in the 0.6–7 keV energy range are ≈1480. A fit to the joint *pn* and MOS spectra with a single power law returns an extremely hard ($\Gamma = -0.44 \pm 0.13$) continuum slope. No useful spectral data can be obtained for the MOS below ≈ 2.5 keV. Line emission is clearly present (Fig. 2) and is best fitted by a neutral ($E = 6.35 \pm 0.04$ keV), strong (rest-frame equivalent width of 2330 ± 520 eV) iron Kα line. The fit quality is statistically acceptable (χ^2/d.o.f. = 36.7/39). A reflection-dominated continuum (*pexrav* model in *xspec* assuming a face on geometry for the reflector with respect to the illuminating source, a cut-off energy of 200 keV for the primary continuum, and solar abundances) plus a Gaussian line well describes the observed spectrum. The intrinsic power law slope ($\Gamma \sim 1.5$) is within the range typical of Seyfert galaxies (i.e. Nandra et al. 1994). The iron line best-fit energy (≃6.4 keV) and equivalent width (≃1.16 keV) are typical of reflection from cold matter (Table 1).

Even though a statistically acceptable fit ($\chi^2 = 32.7/38$) is obtained with an absorbed power law (*plcabs* model in *xspec*), the continuum slope is extremely hard (see Table 1) and unphysical. The flat slope, coupled with the lack of a significant photoelectric cut-off, mimics a reflection-dominated spectrum, which is then considered the best-fit solution. There is no need for additional components to model the soft X-ray continuum (see Fig. 2 and Sect. 3.2). The observed 2–10 keV X-ray flux is about 6.1×10^{-15} erg cm^{-2} s^{-1}, and the corresponding luminosity in the 2–10 keV rest-frame is $\approx 1.8 \times 10^{43}$ erg s^{-1}.

3.2. CXOCDFSJ033229.8-275106 (XID 202) z = 3.70

The *pn* exposure time is about 1892 ks, after flare screening while the average MOS exposure time is about 2720 ks. The source net counts in the 0.4–7.5 keV energy range are ≈1340. A flat slope ($\Gamma = 0.42 \pm 0.10$) is obtained with a single power-law fit to the joint *pn* and MOS spectra. A strong ($EW = 1360 \pm 400$ eV) iron line is clearly detected at a rest frame energy consistent with neutral or mildly ionized iron ($E = 6.55 \pm 0.13$ keV). The fit quality is marginally acceptable (χ^2/d.o.f. = 69.7/44) and is not improved by more complex models for the continuum such as a reflection-dominated spectrum or an absorbed power law (Table 1). In both cases, positive residuals at low energies are present (Fig. 2). If a soft component, modeled with a steep power law, is added to a reflection dominated model for the hard continuum, the fit quality is only marginally improved (see Table 1). On the other hand, a remarkably good fit (χ^2/d.o.f. = 47.1/41) is obtained with a steep spectrum at low energies

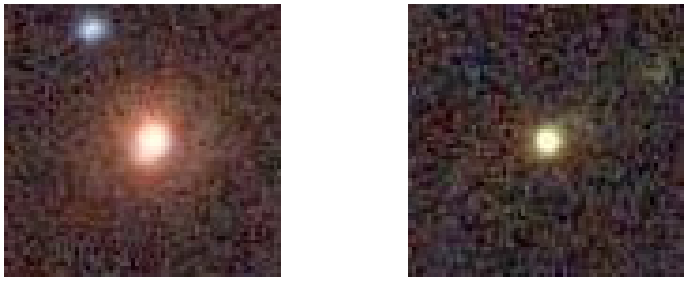

Fig. 3. Color-composite cutouts (2.2 arcsec across, 0.03 arcsec/pixel) from the b, v, i, z HST/ACS observations of GOODS-South (Giavalisco et al. 2004). *Left* XID 153. *Right* XID 202.

plus an absorbed power law at high energies. The best-fit column density of the nuclear, hard X-ray continuum is on the order of 10^{24} cm^{-2}. The soft component accounts for about 0.1% of the unobscured flux at 1 keV. The improvement with respect to an absorbed power law fit without a soft component is highly significant (>99.999%) according to an F-test. Even though the F-test cannot be used to assess the fit quality of models that are not nested, the large difference ($\Delta\chi^2 \simeq$ 20–25 for 1 to 3 degrees of freedom depending form the considered model in Table 1) in the χ^2 statistic allows us to conclude that an absorbed power law plus a soft component is the best-fit solution. To put our findings on solid grounds, given the relatively low signal-to-noise ratio of the observed spectrum, we performed some additional spectral fits. In particular, the parameters of the `pexrav` model are left free to vary in the reflection-dominated plus soft-component fits. The iron abundance and inclination angle of the reflector turned out to be unconstrained by the present data. The fit quality is improved (χ^2/d.o.f $\approx$ 51/41); however, the best-fit parameters are very extreme: $\Gamma \approx 0.58$, $E_{\rm cut} \approx 10$ keV. The flat power-law slope and the low cut-off energy mimic a peaked hard X-ray spectrum with a shape similar to an absorbed power law, thus reinforcing our choice of a heavily absorbed power law as the best-fit model. The observed 2–10 keV flux is $\approx 3.3 \times 10^{-15}$ erg cm^{-2} s^{-1}. Assuming the-best fit parameters (absorbed power law plus soft component), the intrinsic nuclear luminosity in the 2–10 keV rest-frame is $\approx 6 \times 10^{44}$ erg s^{-1}.

4. Discussion

The counting statistics of the *XMM* spectra of the two candidates, high-redshift CT AGN analyzed in this work is of a quality to permit the determination of the presence of heavy absorption in both of them. The relatively bright source at $z = 1.53$ (XID 153) is best described by a reflection-dominated continuum and could be considered as a high-redshift analog of NGC 1068, the Seyfert 2 prototype in the local Universe. The intrinsic X-ray continuum of the $z = 3.70$ type 2 QSO (XID 202) is piercing through a high column density ($\sim 10^{24}$ cm^{-2}) absorber. The very existence of heavily obscured and CT AGN at high redshift, predicted by AGN synthesis models for the XRB and theoretical models for AGN evolution, is confirmed by these deep *XMM-Newton* observations of the CDF-S. Both sources are detected with a number of counts ($\approx$1300–1500) significantly higher than in the 2 Ms *Chandra* observations: about 200 net counts for XID 202 and about 400 for XIS 153 (Bauer et al. in prep.). Also the combined *pn* and MOS signal-to-noise ratio of the *XMM-Newton* data ($\approx$23 and $\approx$19 for XID 153 and XID 202 respectively) is better than for *Chandra* data ($\approx$18 and $\approx$14 for XID 153 and XID 202 respectively), despite the much lower level of the *Chandra* background. A comparable S/N will be achieved with the 4 Ms exposure.

The superior counting statistic of *XMM* data has allowed us to place significantly better constraints on the continuum spectral shape and absorption column densities of the two sources discussed in this paper. While their CT nature was only suspected on the basis of *Chandra* observations, thanks to the deep *XMM-Newton* observations it is now possible to unambiguously confirm the presence of CT circumnuclear matter in both of them and to establish whether the observed X-ray emission is caused by transmission or reflection.

A self-consistent calculation of *Compton*-thick absorption and reprocessing features on the X-ray spectra has been recently published by Murphy & Yaqoob (2009). The authors highlight the need for a proper treatment of absorption and scattering effects when the obscuring gas column density exceeds values on the order of a few 10^{23} cm^{-2}. They also caution against an erroneous interpretation of the parameters obtained by approximate modeling of absorption by CT matter. We have performed spectral fits with the MYTorus model[1] routines available on line (Murphy & Yaqoob 2009).

The best-fit column density of XID 202 ($\approx 1.0^{+0.2}_{-0.1} \times 10^{24}$ cm^{-2}) is perfectly consistent within the errors with that obtained in Table 1. As far as the reflection-dominated fit of XID 153 is concerned, we note that the signal-to-noise of the present data does not allow us to distinguish between the shape predicted by the Murphy & Yaqoob (2009) model and the adopted PEXRAV approximation.

Both objects are optically classified as type 2 AGN on the basis of high-ionization narrow emission lines (Szokoly et al. 2004). Both sources lie in the inner region of the CDF-S area, where deep, multi-wavelength data are available. While the rest-frame UV continuum of XID 202 is very weak and flat, the optical-UV continuum of XID 153 is extremely red ($R-K \simeq 5.7$; Vega magnitudes). The HST cutouts, obtained combining ACS imaging in the b, r, i and z filters, are reported in Fig. 3. The lower redshift object is clearly resolved and shows a spheroidal morphology, while the $z = 3.7$ AGN is pointlike.

It is interesting to compare the broadband properties of these X-ray confirmed CT AGN with some multiwavelength selection criteria proposed to identify heavily obscured AGN at high redshift. The mid-infrared (24 μm) to optical (R band) flux ratio (MIR/O) of XID 153 is ~70, while that of XID 202 is ~200. These values are well below the threshold (MIR/O> 1000) adopted by Fiore et al. (2008) to select high-z candidate obscured AGN. Galaxies showing a mid-IR emission in excess of that expected based on the star-formation rates measured from other multiwavelength data have a very hard *Chandra* stacked spectrum and are likely to host CT nuclei (Daddi et al. 2007). Even if a possible overestimate of the value of the star-formation rate from mid-IR is taken into account (Murphy et al. 2009), both sources would have been selected as mid-IR excess.

Another way to select obscured AGN at relatively high-z is based on the X-ray-to-optical flux ratio (X/O)[2]. A value on the order of 1 or higher is known to be a reliable proxy of optical obscuration (i.e. Fiore et al. 2003). In both sources the measured X/O ratio is relatively high (~0.74 and 0.86 for XID 153 and XID 202 respectively), but well within the distribution observed for X-ray-selected AGN in various surveys.

The two sources presented here would not have been selected as candidate CT AGN by two out of the three multiwavelength criteria discussed above. It should be noted that the efficiency in finding heavily obscured and CT AGN with multiwavelength

[1] `http:://www.mytorus.com`

[2] $X/O = log f_X + R/2.5 + 5.5$ (Hornschemeier et al. 2001).

techniques is very low. Donley et al (2008) pointed out that a selection based on the mid-IR to optical spectral shape is likely to include a significant fraction of dusty, star-forming galaxies. Recently Yaqoob & Murphy (2010) questioned the use of the mid-IR vs X-ray luminosity ratio as a reliable proxy for the column density of obscuring gas. Finally, Silverman et al. (2010) suggest that most of the high X/O ratio sources in the CDF-S are optically obscured, but at moderate $0.5 < z < 1.5$ redshifts.

The full exploitation of the ultra-deep *XMM-Newton* survey in the CDF-S will allow us to uncover the unambiguous signatures of heavy, *Compton*-thick absorption for a sizable sample of relatively X-ray bright sources and, thanks to the extensive multi-wavelength coverage of the field, constrain their broadband spectral energy distributions and validate or devise additional methods for the selection of much fainter sources (Balestra et al., in prep.).

An important question that can be addressed thanks to deep X-ray observations is the distribution of obscuring gas column densities in the *Compton*-thick regime and, in particular, the relative fraction of objects for which the intrinsic nuclear continuum is able to pierce through the obscuring gas, which makes it possible to estimate their nuclear luminosity. These sources are dubbed transmission-dominated or "mildly" *Compton*-thick and are expected to contribute to the hard X-ray background emission. The X-ray spectrum of reflection-dominated or "heavily" CT AGN ($N_{\rm H} \gg 10^{24}$ cm^{-2}, $\tau \gg 1$) is depressed by Compton down-scattering over the entire X-ray band. As a consequence, their contribution to the XRB flux density is likely to be negligible with respect to that of mildly CT AGN. However, they might still be sufficiently numerous to provide a non-negligible contribution to the SMBH mass density.

It is remarkable that previous searches in the CDF-S (Tozzi et al. 2006) and CDF-N (Georgantopoulos et al. 2009) seem to suggest that reflection-dominated sources are much more abundant than "mildly" CT AGN (i.e. 9 out of the 10 candidates in the CDF-N and all 14 candidates in the CDF-S were considered to be reflection-dominated, though the present results indicate that XID 202 at least is not). However, given that CT candidates in the *Chandra* deep fields are identified on the basis of a flat hard X-ray spectrum, a strong bias toward reflection-dominated AGN is likely to be present in these *Chandra* samples. We expect to detect and recognize about 30–40 CT AGN in the CDF-S. About 30–40% of them (Gilli et al. 2007) will be detected with a number of counts comparable to the two presented here. The obscuring column density will be measured with an accuracy that is good enough to distinguish between heavy absorption and reflection.

5. Conclusions

The spectral capabilities of the *pn* and MOS camera onboard *XMM-Newton* coupled with an ultra-deep exposure fully meet the expectation and are providing high quality X-ray spectra, which will allow us to address several important aspects concerning the physics and the evolution of the most obscured AGN. As an example of the quality of the future results that can be obtained with these data, we showed that

- The *XMM-Newton* deep exposure in the CDF-S allowed us to obtain good quality X-ray spectra of two high-redshift AGN, which are suspected to host a CT nucleus on the basis of *Chandra* observations.
- The high-energy emission of the $z = 3.7$ AGN is obscured by cold matter with a column density close to but slightly lower ($\tau \approx 0.7$) than unit optical depth for Compton scattering. Reflection from a *Compton*-thick reprocessor is the most likely explanation for the very hard X-ray spectrum of the $z = 1.53$ source.
- The comparison with some of the multiwavelength criteria, devised for the selection of *Compton*-thick AGN at high redshift, highlights the importance of deep X-ray observations for a robust determination of the obscuring gas properties.

Acknowledgements. The authors would like to warmly thank Maria Diaz Trigo and Ignacio della Calle for their valuable help and advice in the scheduling of the *XMM*-CDF-S observations. Support from the Italian Space Agency (ASI) under the contracts ASI-INAF I/088/06/0 and I/009/10/0 is acknowledged. A.C. acknowledges the NASA grant NNX09AQ05G to visit CfA, where part of this work was written. I.G. and A.C. acknowledge the Marie Curie fellowship FP7-PEOPLE-IEF-2008 Prop. 235285. X.B. and F.J.C. acknowledge financial support from the Spanish Ministerio de Ciencia e Innovación under project AYA2009-08059. M.B. acknowledges support by the Deutsches Zentrum für Luft- und Raumfahrt, DLR project numbers 50 OR 0207 and 50 OR 0405. F.C., F.N. and M.B. acknowledge NASA grants NNX08AX51G and NNX09AQ05G. F.C. acknowledges support from the Blanceflor Boncompagni Ludovisi Foundation. J.D.S. is supported by World Premier International (WPI) Research Center Initiative , MEXT, Japan. W.N.B. acknowledges NASA grant SV0-80004 and NASA ADP grant NNX10AC99G. F.E.B. cknowledges the support of CONICYT, Chile, under grants FONDECYT 1101024 and FONDAP (CATA) 15010003.

References

Alexander, D. M., Bauer, F. E., Brandt, W. N., et al. 2003, AJ, 126, 539
Alexander, D. M., Chary, R.-R., Pope, A., et al. 2008, ApJ, 687, 835
Beckmann, V., Soldi, S., Ricci, C., et al. 2009, A&A, 505, 417
Comastri, A., 2004, in Supermassive Black Holes in the Distant Universe, ed. A.J. Barger (Kluwer Academic Publishers), 245
Comastri, A., Gilli, R.,& Hasinger, G. 2005, Exp. Astron., 20, 41
Daddi, E., Alexander, D. M., Dickinson, M., et al. 2007 ApJ, 670 173
Della Ceca, R., Severgnini, P., Caccianiga, A., et al. 2008, MemSait, 79, 65
Donley, J. L., Rieke, G. H., Pérez-González, P. G., & Barro, G. 2008, ApJ, 687, 111
Fiore, F., Brusa, M., Cocchia, F., et al. 2003, A&A, 409, 79
Fiore, F., Grazian, A., Santini, P., et al. 2008, ApJ, 672, 94
Fiore, F., Puccetti, S., Brusa, M., et al. 2009 ApJ, 693, 447
Georgantopoulos, I., Akylas, A., Georgakakis, A., & Rowan-Robinson M. 2009, A&A, 507, 747
Giacconi, R., Zirm, A., Wang, J. X., et al. 2002, ApJS, 139, 369
Giavalisco, M., Ferguson, H. C., Koekemoer, A. M., et al. 2004, ApJ, 600, L93
Gilli, R., Comastri A., & Hasinger, G. 2007, A&A, 463, 79
Gilli, R., Vignali, C., & Mignoli, M., et al. 2010, A&A, 519, A92
Guainazzi, M., Matt G., & Perola G. C. 2005, A&A, 444, 119
Hopkins, P. F., Hernquist, L., Cox, T. J., et al. 2006, ApJS, 163, 1
Iwasawa, K., Crawford, C. S., Fabian, A. C., & Wilman, R. J. 2005, MNRAS, 362, L20
Luo, B., Bauer, F. E., Brandt, W. N., et al. 2008, ApJS, 179, 19
Marconi, A., Risaliti, G., Gilli, R., et al. 2004, MNRAS, 351, 169
Menci, N., Fiore, F., Puccetti S., & Cavaliere, A. 2008, ApJ, 686, 219
Murphy, E. J., Cohen, A. B., Ravoori, B., et al. 2009, ApJ, 698, 138
Murphy, K. D., & Yaqoob, T. 2009, MNRAS, 397, 1549
Nandra, K., Coil, A. L., Georgakakis, A., et al. 1994, ApJ, 477, 602
Norman, C., Hasinger, G., Giacconi, R., et al. 2002, ApJ, 571, 218
Page, M. J., Stevens, J. A., Ivison, R. J., & Carrera, F. J. 2004, ApJ, 611, L85
Risaliti, G., Maiolino, R., Salvati, M., et al. 1999, ApJ, 522, 157
Silverman, J. D., Mainieri, V., Salvato, M., et al. 2010, ApJS, 191, 124
Szokoly, G. P., Bergeron, J., Hasinger, G., et al. 2004, ApJS, 155, 271
Tozzi, P., Gilli, R., Mainieri, V., et al. 2006, A&A, 451, 457
Treister, E., & Urry, C. M. 2005, ApJ, 630, 115
Treister, E., Urry, C. M., & Virani S. 2009, ApJ, 696, 110
Tueller, J., Baumgartner, W. H., Markwardt, C. B., et al. 2010, ApJS, 186, 378
Vignali, C., Alexander, D. M., Gilli R., & Pozzi F. 2010, MNRAS, 404, 48
Worsley, M.A., Fabian, A.C., Barcons X., et al., 2004, MNRAS, 352, L28
Yaqoob, T., & Murphy, K. D. 2010, MNRAS, in press [arXiv:1010.6077]

Table 1. Best-fit parameters for reflection-dominated and transmission-dominated models.

Source ID	Model[a]	Γ	Γ_S[b]	N_H 10^{22} cm^{-2}	$E_{K\alpha}$ keV	EW[c] eV	χ^2/d.o.f
153	**REF**	1.50 ± 0.10	...	...	$6.36^{+0.07}_{-0.05}$	1160^{+440}_{-350}	28.9/39
153	ABS	-0.11 ± 0.22	...	$5.0^{+3.5}_{-2.1}$	6.35 ± 0.04	1870^{+410}_{450}	32.7/38
202	REF	1.99 ± 0.10	...	...	6.57 ± 0.13	760^{+340}_{-250}	72.4/44
202	PL+REF	1.95 ± 0.10	$7.3^{+0.4}_{-0.6}$	...	6.57 ± 0.13	930^{+300}_{-330}	60.9/42
202	ABS	$1.48^{+0.33}_{-0.40}$	...	58^{+32}_{-22}	6.54 ± 0.15	840^{+290}_{-470}	69.4/43
202	**PL+ABS**	$1.82^{+0.34}_{-0.59}$	$4.1^{+0.5}_{-0.9}$	88^{+68}_{-40}	6.53 ± 0.14	840 ± 320	47.1/41

Notes. Errors are at 1σ. The best fit model is in boldface in Col. 2. [(a)] Fitted models: reflection-dominated (REF), absorbed power-law (ABS), power law plus absorbed power-law (PL+ABS). [(b)] Γ_S is the power-law slope of the soft component. [(c)] The iron line EW with respect to the intrinsic (unabsorbed) continuum is ≈1660 eV for XID 153 and ≈160 eV for XID 202.